

Collaborative Low-Rank Adaptation for Pre-Trained Vision Transformers

Zheng Liu, Jinchao Zhu, and Gao Huang, *Member, IEEE*

Abstract—Low-rank adaptation (LoRA) has achieved remarkable success in fine-tuning pre-trained vision transformers for various downstream tasks. Existing studies mainly focus on exploring more parameter-efficient strategies or more effective representation learning schemes. However, these methods either sacrifice fine-tuning performance or introduce excessive trainable parameters, failing to strike a balance between learning performance and parameter efficiency. To address this problem, we propose a novel tuning method named collaborative low-rank adaptation (CLoRA) in this paper. CLoRA consists of base-space sharing and sample-agnostic diversity enhancement (SADE) components. To maintain parameter efficiency while expanding the learning capacity of low-rank modules (LRMs), base-space sharing allows all LRMs to share a set of down/up-projection spaces. In CLoRA, the low-rank matrices obtained from the shared spaces collaboratively construct each LRM. Since the representations extracted by these matrices may contain redundant information, SADE is employed to regularize the similarities among them to encourage diverse representations in the training process. We conduct extensive experiments on widely used image and point cloud datasets to evaluate the performance of CLoRA. Experimental results demonstrate that CLoRA strikes a better balance between learning performance and parameter efficiency, while requiring the fewest GFLOPs for point cloud analysis, compared with the state-of-the-art methods.

Index Terms—Parameter-efficient fine-tuning, low-rank adaptation, vision transformers, diversity enhancement.

I. INTRODUCTION

VISION transformers (ViTs) [1] have attained significant success across various computer vision tasks [2], [3], [4]. However, the strong performance relies on large amounts of training data. Consequently, a high-performing ViT is difficult to train from scratch in data-scarce scenarios [5]. To overcome the difficulty, a prevalent strategy is to first pre-train a ViT on large-scale datasets and subsequently fine-tune the entire model for target domains [6], [7]. Nevertheless, the strategy requires storing one entire ViT model for each downstream task, resulting in substantial storage costs.

Parameter-efficient fine-tuning (PEFT) [8], [9], [10] has become an active research area aimed at addressing the above challenge. Unlike full fine-tuning, PEFT methods, such as adapter [11], prompt learning [12], and low-rank adaptation (LoRA) [13], normally introduce only a small number of trainable parameters while keeping the backbone model frozen.

Z. Liu is with the School of Automation and Electrical Engineering, University of Science and Technology Beijing, Beijing 100083, China, and also with the Beijing Engineering Research Center of Industrial Spectrum Imaging, Beijing 100083, China. J. Zhu is with the College of Software, Nankai University, Tianjin 300350, China. G. Huang is with the Department of Automation, BNRist, Tsinghua University, Beijing 100084, China.

Corresponding author: J. Zhu (e-mail: jczhu@nankai.edu.cn).

Among these methods, LoRA has attracted increasing attention from researchers and has been broadly discussed in recent years [14], [15], [16].

Given a set of pre-trained weights $\{\mathbf{W}_i\}_{i=1}^m$ in a pre-trained backbone, where m denotes the number of weights, LoRA assumes that their weight updates $\{\Delta\mathbf{W}_i\}_{i=1}^m$ are low-rank and can be learned by multiplying the corresponding low-rank down-projection matrices $\{\mathbf{A}_i\}_{i=1}^m$ and up-projection matrices $\{\mathbf{B}_i\}_{i=1}^m$. During the fine-tuning process, LoRA adopts m low-rank modules (LRMs) to capture the updates of $\{\mathbf{W}_i\}_{i=1}^m$. As for the j -th LRM, its input is first projected into a low-dimensional space with dimension r by down-projection matrix \mathbf{A}_j and then is remapped back to the original space by up-projection matrix \mathbf{B}_j . After training, by substituting \mathbf{W}_j with $\mathbf{W}_j + \mathbf{A}_j\mathbf{B}_j$, LoRA keeps the structural integrity of the original backbone. As numerous weights exist in a transformer-based backbone, applying LRMs to all of them would significantly increase the number of trainable parameters. Hence, LoRA typically employs LRMs to learn the updates of query and value projection weights. In ViT, each encoder layer primarily consists of a multi-head attention (MHA) block and a feed-forward network (FFN) block. However, LoRA may perform poorly on some downstream tasks because it only adapts a limited subset of the MHA blocks (query and value projection weights) while ignoring the FFN blocks. A related method named ARC [17] experimentally demonstrates that adapting the inputs to MHA and FFN blocks is more effective than updating the query and value projection weights, when tuning pre-trained ViT backbones to downstream tasks. Note that each tuned weight in ARC can be viewed as an identity matrix \mathbf{I} with proper size. Taking the j -th LRM as an example, we show the tuning difference between LoRA and ARC in Fig. 1.

As illustrated by existing LoRA-based studies [14], [15], r significantly affects the expressive power of LRMs, and it is hard to achieve satisfactory fine-tuning results with small r . There are two widely used approaches to solve this problem. The first one is directly enlarging the value of r [18]. The second one is employing a group of low-rank matrices to learn the weight update in each inserted LRM [19]. However, both approaches introduce a large number of trainable parameters, which may lead to overfitting during fine-tuning. This raises the question: is it necessary to improve the fine-tuning performance by substantially increasing the number of trainable parameters? Upon closer examination, both methods essentially increase the rank upper bound of weight updates, which indicates that expanding the rank capacity is a feasible way to enhance the learning abilities of LRMs.

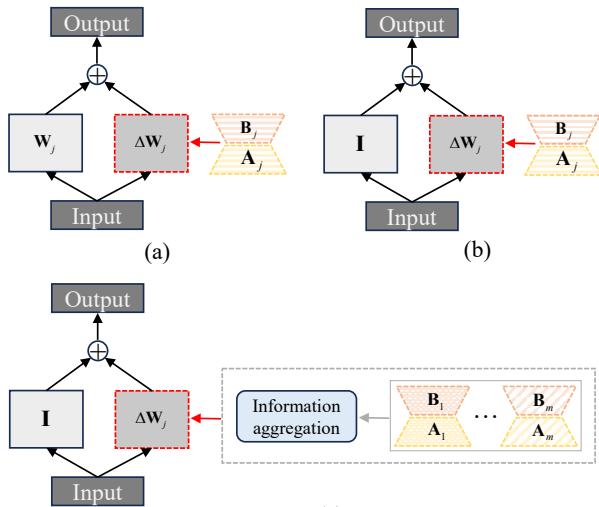


Fig. 1. Low-rank structures of (a) LoRA, (b) ARC, and (c) CLoRA.

In LoRA, m LRM s are independent of each other and the rank upper bound of each low-rank matrix is r . According to the subadditivity of matrix rank, we observe that the rank upper bound of $\sum_{i=1}^m \mathbf{A}_i \mathbf{B}_i$ is larger than r . This suggests that it is possible to enhance the learning capacity of each injected module without introducing extra parameters by exploiting the low-rank matrices contained in the others. Based on this observation, we present a simple but effective method termed as collaborative low-rank adaptation (CLoRA) for pre-trained ViTs. As shown in Fig. 1, for the j -th LRM, CLoRA utilizes the information contained in all low-rank matrices $\{\mathbf{A}_i \mathbf{B}_i\}_{i=1}^m$ to collaboratively learn $\Delta \mathbf{W}_j$, whereas LoRA and ARC rely solely on the individual information in $\mathbf{A}_j \mathbf{B}_j$.

CLoRA consists of base-space sharing and sample-agnostic diversity enhancement (SADE) components. Under base-space sharing, $\{\Delta \mathbf{W}_i\}_{i=1}^m$ of all LRM s are collaboratively constructed by $\{\mathbf{A}_i\}_{i=1}^m$ and $\{\mathbf{B}_i\}_{i=1}^m$ which share the same base down-projection and up-projection spaces, respectively. Since each LRM in CLoRA combines multiple low-rank projection matrices, SADE is designed to enhance the diversity of the representations obtained by these projection matrices. The main contributions are as follows.

- We present an effective base-space sharing scheme to combine the information contained in $\{\mathbf{A}_i\}_{i=1}^m$ and $\{\mathbf{B}_i\}_{i=1}^m$ during the learning process of each LRM, which significantly improves the learning capacity of LRM s and decreases the parameter count.
- To mitigate redundant information in the representations extracted from multiple low-rank matrices within each LRM, SADE efficiently regularizes the similarities among these representations during training.
- Extensive experiments on widely used image and point cloud datasets demonstrate the superiority of CLoRA over the state-of-the-art methods.

II. RELATED WORK

In recent years, parameter-efficient fine-tuning (PEFT) has emerged as a dominant approach for transferring the generalizable knowledge embedded in pre-trained transformer backbones to diverse downstream tasks. The mainstream studies can be roughly partitioned into five categories: prompt tuning, adapter tuning, reparameterization tuning, side-tuning, and hybrid tuning.

Prompt tuning inserts extra learnable prompts into pre-trained backbones to capture task-specific information [20]. For example, Jia et al. [12] prepend a set of trainable tokens to either the first encoder layer only or all encoder layers; Pei et al. [21] learn two-dimensional prompt maps with sizes matching the corresponding image token maps for encoder layers; Hu et al. [22] and Zhang et al. [23] aggregate the intermediate information of pre-trained backbones by adding additional tokens for the queries in MHA blocks; Nie et al. [24] first divide the pre-trained backbone into multiple stages and then construct stage-wise prompt blocks to generate task-specific discriminative prompts for downstream task inputs. **Adapter tuning** inserts trainable bottleneck modules into pre-trained backbones, where each module comprises a down-projection layer, a non-linear activation, and an up-projection layer [25], [26]. Adapter-based methods typically extract downstream task-specific representations by applying these modules to 1) learn the supplementary information for FFN blocks [27], [28] or additional transformer components [29] and 2) transform the input or output representations of core building blocks such as MHA and FFN blocks [30], [31]. **Side-tuning** trains a separate lightweight side network in parallel with the frozen pre-trained backbone and fuses their outputs for final predictions [32]. Such side networks either integrate the features extracted from the pre-trained backbone sequentially [33], [34] or fuse the extracted features through parallel aggregation [35], [36]. Unlike the above three categories which usually bring extra inference costs, **reparameterization tuning** aims to avoid the inference overhead by tuning the parameters that are either part of the backbone or can be merged into the backbone weights after training [37]. Methods belonging to this category design some strategies to identify task-specific parameters [38] or apply the modules with linear structures that can be incorporated into existing layers to learn task-specific representations [39], [40]. **Hybrid tuning** combines methods from different categories. For example, Zhou et al. [41] inject prompt tokens and dynamic adapters into encoder layers; Zhang et al. [42] explore the optimal combination of adapters, learnable tokens and linear LRM s by neural architecture search techniques.

Owing to its ability to avoid extra computational overhead, reparameterization tuning has received growing interest in the deep learning community. As a representative method, LoRA [13] has been widely studied. LoRA assumes that the weight updates for downstream tasks can be captured by linear LRM s where each of them consists of a down-projection matrix (mapping inputs into a low space with dimension r) and an up-projection matrix (remapping subspace embeddings back to the original space). Most existing studies focus on exploring

effective strategies to learn representative down-projection and up-projection matrices. For example, Liu et al. [14] divide pre-trained weights into magnitude and direction components and LRM are employed to learn directional updates; Hayou et al. [43] assign different learning rates for down-projection and up-projection matrices; Lin et al. [44] learn projection matrices based on the singular value decomposition of pre-trained weights; Yang et al. [45] employ two vectors to dynamically generate down-projection and up-projection matrices. When the pre-trained weights for LRM are set as identity matrices, these modules are normally adopted to adapt the inputs of some components (such as MHA and FFN blocks) contained in pre-trained backbones [17], [46]. In practice, r has a significant influence on the performance of LoRA-based methods. A small r usually results in poor learning abilities [14], [15] while a large r greatly increases the number of trainable parameters. Currently, motivated by the success of mixture of experts (MoE) [47], some researchers have begun to design strategies to combine multiple experts in LRM where each expert is composed of a pair of down-projection and up-projection matrices. MOLE [48] employs learnable gating functions to compose multiple experts. In HydraLoRA [49], all experts in each LRM share the same down-projection matrix. LoRAMoE [50] assigns multiple experts to learn task-specific information for FFN blocks. However, these methods introduce extra inference overhead due to the nonlinear routers used to evaluate the contribution of experts. To preserve the original property of LoRA, some studies [19], [50] treat different experts equally.

Enlarging the value of r and combining multiple experts (a pair of down-projection and up-projection matrices) in LRM are two effective ways to enhance the fine-tuning performance of LoRA-based methods. Both ways expand the rank upper bound of learned low-rank matrices, indicating that increasing the rank upper bound is a feasible approach to improve the learning abilities of these LRM. Unfortunately, they bring a large number of trainable parameters, resulting in a parameter-inefficiency problem. Our proposed method (CLORA) also incorporates multiple experts, but it is much more parameter-efficient than existing LoRA-based ensemble methods due to the designed base-space sharing scheme. Besides, during the training process, CLORA encourages learning diverse experts by regularizing the similarities among the representations extracted by these experts, which is usually ignored by existing methods.

III. PRELIMINARIES

A. Vision Transformer

The architecture of a standard vision transformer (ViT) [1] is composed of a patch embedding layer, L stacked encoder layers, and a prediction head.

In ViT, the patch embedding layer is employed to transform input images into suitable embeddings for the subsequent layers. Specifically, given an input image $\mathbf{X} \in R^{h \times w \times 3}$, it first converts \mathbf{X} into a sequence of n flattened patches $[\mathbf{x}_1; \dots; \mathbf{x}_n] \in R^{n \times 3m^2}$ and then obtains embedding tokens $[\mathbf{x}_1\mathbf{W}; \dots; \mathbf{x}_n\mathbf{W}] \in R^{n \times d}$ with mapping matrix $\mathbf{W} \in$

$R^{3m^2 \times d}$, where (h, w) and (m, m) are the resolutions of \mathbf{X} and its patches, d is the dimension of each token, and $n = \frac{hw}{m^2}$. The mathematical expression of this layer is formulated as

$$\mathbf{Z}^0 = [\mathbf{x}_{class}; \mathbf{x}_1\mathbf{W}; \dots; \mathbf{x}_n\mathbf{W}] + \mathbf{E}_{pos}, \quad (1)$$

where $\mathbf{x}_{class} \in R^{1 \times d}$ is the prepended class token, $\mathbf{E}_{pos} \in R^{(n+1) \times d}$ denotes the position embeddings of tokens and \mathbf{Z}^0 represents the transformed token set of this layer.

Encoder layers inserted after the patch embedding layer are designed to process the output information \mathbf{Z}^0 . Each encoder layer consists of a MHA block and a FFN block, where each of them is preceded by a layer normalization (LN) module. As for the l -th ($1 \leq l \leq L$) encoder layer, its mathematical expression is

$$\tilde{\mathbf{Z}}^l = \text{MHA}(\text{LN}(\mathbf{Z}^{l-1})) + \mathbf{Z}^{l-1}, \quad (2)$$

$$\mathbf{Z}^l = \text{FFN}(\text{LN}(\tilde{\mathbf{Z}}^l)) + \tilde{\mathbf{Z}}^l, \quad (3)$$

where $\tilde{\mathbf{Z}}^l$ and \mathbf{Z}^l denote the outputs of the MHA and FFN blocks. Note that \mathbf{Z}^l is also the output of the encoder layer.

Through equations (1)-(3), we can calculate the class token's representation at the L -th encoder layer. Let \mathbf{z}_{class}^L denote the representation of \mathbf{x}_{class} contained in \mathbf{Z}^L , the prediction result \mathbf{y} for \mathbf{X} is

$$\mathbf{y} = \text{PH}(\text{LN}(\mathbf{z}_{class}^L)), \quad (4)$$

where $\text{PH}(\cdot)$ represents a lightweight classifier.

B. Low-Rank Adaptation

LoRA [13] is based on the hypothesis that weight updates lie in low-rank spaces when adapting a pre-trained backbone to downstream tasks.

When fine-tuning a ViT backbone with LoRA, the updated weights are typically $d \times d$ matrices. Therefore, for the j -th LRM, we have $\mathbf{W}_j \in R^{d \times d}$ and $\Delta\mathbf{W}_j \in R^{d \times d}$. As shown in Fig. 1(a), $\Delta\mathbf{W}_j$ is parameterized as $\mathbf{A}_j\mathbf{B}_j$ to ensure the low-rank property, where $\mathbf{A}_j \in R^{d \times r}$ and $\mathbf{B}_j \in R^{r \times d}$ are down-projection and up-projection matrices. In the j -th LRM, the output representation \mathbf{X}_{output}^j is obtained by

$$\mathbf{X}_{output}^j = \mathbf{X}_{input}^j(\mathbf{W}_j + \Delta\mathbf{W}_j) = \mathbf{X}_{input}^j(\mathbf{W}_j + \mathbf{A}_j\mathbf{B}_j), \quad (5)$$

where \mathbf{X}_{input}^j is the input of this module.

During the fine-tuning process, LoRA freezes the weights $\{\mathbf{W}_i\}_{i=1}^m$ and only trains $\{\mathbf{A}_i\mathbf{B}_i\}_{i=1}^m$ with the data from downstream tasks. Compared with full fine-tuning, LoRA greatly reduces the number of trainable parameters. At the inference stage, $\{\mathbf{A}_i\mathbf{B}_i\}_{i=1}^m$ can be directly merged into the corresponding weights through replacing $\{\mathbf{W}_i\}_{i=1}^m$ with $\{\mathbf{W}_i + \mathbf{A}_i\mathbf{B}_i\}_{i=1}^m$, avoiding additional computational and storage costs.

IV. COLLABORATIVE LOW-RANK ADAPTATION

Inspired by the work of LoRA [13] and ARC [17], we show the architecture of CLORA in Fig. 2. As displayed, two low-rank modules (LRMs) are employed to adapt the input representations of the MHA and FFN blocks in each encoder layer, respectively. To reduce the number of trainable

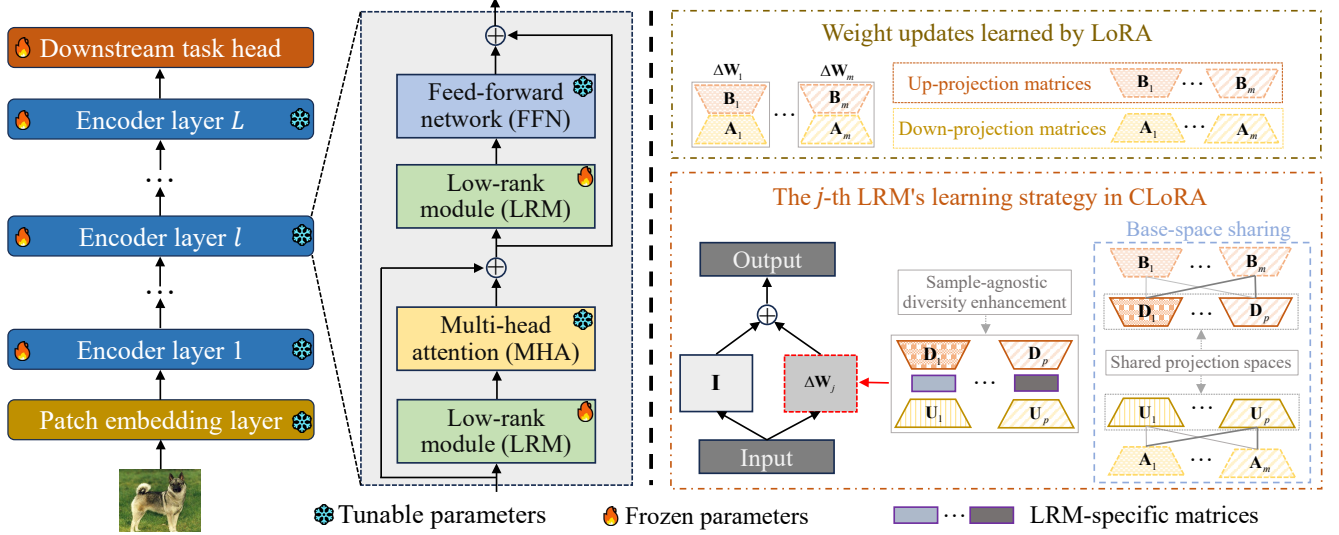


Fig. 2. Illustration of CLoRA. In LoRA, LRMs are applied to adapt the input representations of MHA and FFN blocks, yielding $\{\Delta\mathbf{W}_i = \mathbf{A}_i\mathbf{B}_i\}_{i=1}^m$, where $\{\mathbf{A}_i\mathbf{B}_i\}_{i=1}^m$ are independent of each other. By contrast, each LRM in CLoRA effectively and efficiently utilizes the information contained in $\{\mathbf{A}_i\mathbf{B}_i\}_{i=1}^m$ through the base-space sharing and SADE components.

parameters and simultaneously increase the rank upper bounds of $\{\Delta\mathbf{W}_i\}_{i=1}^m$, we introduce a novel base-space sharing scheme where $\{\Delta\mathbf{W}_i\}_{i=1}^m$ are collaboratively parameterized by down/up-projection matrices ($\{\mathbf{A}_i\}_{i=1}^m/\{\mathbf{B}_i\}_{i=1}^m$) which share common down/up-projection spaces. Specifically, each of $\{\mathbf{A}_i\}_{i=1}^m$ (or $\{\mathbf{B}_i\}_{i=1}^m$) can be linearly represented by shared down-projection matrices $\{\mathbf{D}_h\}_{h=1}^p$ (or up-projection matrices $\{\mathbf{U}_h\}_{h=1}^p$), where $p < m$. Under this scheme, $\{\Delta\mathbf{W}_i\}_{i=1}^m$ are learned via LRM-specific matrices and the shared down/up-projection matrices. As a result, each of $\{\Delta\mathbf{W}_i\}_{i=1}^m$ is the combination of multiple low-rank projection matrices. Finally, sample-agnostic diversity enhancement (SADE) is designed to improve the quality of $\{\Delta\mathbf{W}_i\}_{i=1}^m$ by regularizing the similarities among the representations extracted by these matrices during training.

A. Base-Space Sharing

When LRMs in LoRA are employed to tune the input representations of MHA and FFN blocks, as in ARC, the tuned weights in pre-trained backbones can be viewed as identity matrices. Correspondingly, for the j -th LRM, its output \mathbf{X}_{output}^j can be obtained by

$$\mathbf{X}_{output}^j = \mathbf{X}_{input}^j(\mathbf{I} + \Delta\mathbf{W}_j) = \mathbf{X}_{input}^j + \mathbf{X}_{input}^j \mathbf{A}_j \mathbf{B}_j. \quad (6)$$

The above equation indicates that the transformed representation \mathbf{X}_{output}^j is the sum of the original representation and its update. In this case, the update of \mathbf{X}_{input}^j is learned by low-rank matrix $\mathbf{A}_j \mathbf{B}_j$. Since $r \ll d$, we have $rank(\mathbf{A}_j \mathbf{B}_j) \leq r$ where $rank(\cdot)$ represents the rank of $\mathbf{A}_j \mathbf{B}_j$. r is an essential hyper-parameter for LoRA. In practice, a small r usually limits the fine-tuning abilities on pre-trained models, while a large r can bring numerous trainable parameters, resulting in parameter inefficiency. Actually, r affects the fine-tuning performance by controlling the upper bound of $\Delta\mathbf{W}_j$'s rank.

A small (or large) r means a low (or high) upper bound on the rank. If r is set as a small value, the learned low-rank space may have difficulty approximating the actual low-rank space, because the rank upper bound is limited. Therefore, enlarging the upper bound of rank is a feasible way to enhance the fine-tuning performance when r is small.

In LoRA-based tuning methods, low-rank matrices $\{\mathbf{A}_i \mathbf{B}_i\}_{i=1}^m$ inserted into pre-trained backbones are applied to extract different representations and $\{\mathbf{A}_i \mathbf{B}_i\}_{i=1}^m$ are normally different. Since $rank(\sum_{i=1}^m \mathbf{A}_i \mathbf{B}_i) \leq \sum_{i=1}^m rank(\mathbf{A}_i \mathbf{B}_i) \leq mr$, if we properly utilize all the inserted low-rank matrices, the rank upper bound can be increased to mr , thus improving the fine-tuning abilities. A simple idea is to learn each representation update by $\{\mathbf{A}_i \mathbf{B}_i\}_{i=1}^m$. For example, in the j -th LRM, the output \mathbf{X}_{output}^j is formulated as

$$\mathbf{X}_{output}^j = \mathbf{X}_{input}^j(\mathbf{I} + \Delta\mathbf{W}_j) = \mathbf{X}_{input}^j + \mathbf{X}_{input}^j \sum_{i=1}^m \mathbf{A}_i \mathbf{B}_i. \quad (7)$$

For the m LRMs at different locations, their input representation updates usually have different requirements for $\{\mathbf{A}_i \mathbf{B}_i\}_{i=1}^m$, indicating that some optimization conflicts may exist in the whole tuning process. To avoid the potential problem, we design LRM-specific transformation matrices $\{\Lambda_{i,j}\}_{i=1}^m$ for $\Delta\mathbf{W}_j$ and then reformulate equation (7) as

$$\mathbf{X}_{output}^j = \mathbf{X}_{input}^j + \mathbf{X}_{input}^j \sum_{i=1}^m \mathbf{A}_i \Lambda_{i,j} \mathbf{B}_i, \quad (8)$$

where $\Lambda_{i,j} \in R^{r \times r}$ is $\Delta\mathbf{W}_j$'s specific transformation matrix used to utilize the information contained in $\mathbf{A}_i \mathbf{B}_i$. Note that $\Lambda_{i,j} = \mathbf{I}$ if $j = i$.

However, equation (8) will introduce more trainable parameters than those of LoRA. To lower the introduced parameter count, we assume that $\{\mathbf{A}_i \mathbf{B}_i\}_{i=1}^m$ share the same low-rank

spaces $\{S_h\}_{h=1}^p$ ($p < m$). Under this assumption, each of $\{\mathbf{A}_i \mathbf{B}_i\}_{i=1}^m$ can be divided into multiple component matrices in spaces $\{S_h\}_{h=1}^p$. We denote the component matrices for \mathbf{A}_i and \mathbf{B}_i in the h -th low-rank space S_h as \mathbf{A}_i^h and \mathbf{B}_i^h . Suppose space S_h can be represented by $\mathbf{D}_h \mathbf{U}_h$, where \mathbf{D}_h and \mathbf{U}_h denote the base down-projection and up-projection matrices, respectively. Assuming matrices $\mathbf{T}_i^h \in R^{r \times r}$ and $\mathbf{R}_i^h \in R^{r \times r}$ are the representations for \mathbf{A}_i^h and \mathbf{B}_i^h under base projection matrices \mathbf{D}_h and \mathbf{U}_h , we have $\mathbf{A}_i^h = \mathbf{D}_h \mathbf{T}_i^h$ and $\mathbf{B}_i^h = \mathbf{R}_i^h \mathbf{U}_h$. Accordingly, we have $\mathbf{A}_i = \sum_{h=1}^p \mathbf{A}_i^h = \sum_{h=1}^p \mathbf{D}_h \mathbf{T}_i^h$ and $\mathbf{B}_i = \sum_{h=1}^p \mathbf{B}_i^h = \sum_{h=1}^p \mathbf{R}_i^h \mathbf{U}_h$. Similarly, we also divide $\Delta \mathbf{W}_j$ into multiple component matrices in spaces $\{S_h\}_{h=1}^p$. For $\Delta \mathbf{W}_j$, its component matrix $\Delta \mathbf{W}_j^h$ in space S_h is obtained as follows.

$$\Delta \mathbf{W}_j^h = \sum_{i=1}^m \mathbf{A}_i^h \mathbf{\Lambda}_{i,j}^h \mathbf{B}_i^h = \sum_{i=1}^m \mathbf{D}_h \mathbf{T}_i^h \mathbf{\Lambda}_{i,j}^h \mathbf{R}_i^h \mathbf{U}_h, \quad (9)$$

where $\mathbf{\Lambda}_{i,j}^h$ is the corresponding component of $\mathbf{\Lambda}_{i,j}$ in space S_h .

Based on equation (9), we have

$$\Delta \mathbf{W}_j = \sum_{h=1}^p \Delta \mathbf{W}_j^h = \sum_{h=1}^p \mathbf{D}_h \mathbf{Q}_i^h \mathbf{U}_h, \quad (10)$$

where $\mathbf{Q}_i^j = \sum_{i=1}^m \mathbf{T}_i^h \mathbf{\Lambda}_{i,j}^h \mathbf{R}_i^h$.

As analyzed above, the output of the j -th LRM in CLoRA is formulated as

$$\mathbf{X}_{output}^j = \mathbf{X}_{input}^j + \mathbf{X}_{input}^j \sum_{h=1}^p \mathbf{D}_h \mathbf{Q}_i^h \mathbf{U}_h. \quad (11)$$

All components in \mathbf{Q}_i^j are trainable during the fine-tuning process, which implies \mathbf{Q}_i^j is also trainable. In equation (11), we can directly train a suitable \mathbf{Q}_i^j using the data of downstream tasks and thus ignore the learning processes of its components.

As shown in Fig. 2, two LRMs are inserted before the MHA and FFN blocks of each encoder layer. Taking the l -th encoder layer as an example, the $(2l-1)$ -th and $2l$ -th LRMs are inserted in this layer. Let $\tilde{\mathbf{Z}}_{MHA}^l$ and $\tilde{\mathbf{Z}}_{FFN}^l$ denote the transformed inputs for the MHA and FFN blocks, based on equations (1-3,11), we have

$$\tilde{\mathbf{Z}}_{MHA}^l = \text{LN}(\mathbf{Z}^{l-1}) + \text{LN}(\mathbf{Z}^{l-1}) \sum_{h=1}^p \mathbf{D}_h \mathbf{Q}_i^{2l-1} \mathbf{U}_h, \quad (12)$$

$$\mathbf{Z}_{FFN}^l = \text{LN}(\tilde{\mathbf{Z}}^l) + \text{LN}(\tilde{\mathbf{Z}}^l) \sum_{h=1}^p \mathbf{D}_h \mathbf{Q}_i^{2l} \mathbf{U}_h. \quad (13)$$

Finally, the mathematical expressions of the MHA and FFN blocks become

$$\tilde{\mathbf{Z}}^l = \text{MHA}(\tilde{\mathbf{Z}}_{MHA}^l) + \mathbf{Z}^{l-1}, \quad (14)$$

$$\mathbf{Z}^l = \text{FFN}(\mathbf{Z}_{FFN}^l) + \tilde{\mathbf{Z}}^l. \quad (15)$$

During the fine-tuning stage, we freeze the parameters of the original backbone and only update the parameters contained

in LRMs and the prediction head using the data of each downstream task. In the above way, the total number of introduced extra parameters is $(2dr + mr^2)p + c$, where c represents the number of parameters in the prediction head. In LoRA, the number of extra trainable parameters is $2drm + c$. Since $r \ll d$ and $p < m$, we have $(2dr + mr^2)p + c \approx 2drp + c < 2drm + c$. Although $\text{rank}(\sum_{h=1}^p \mathbf{D}_h \mathbf{Q}_i^h \mathbf{U}_h) \leq pr < mr$, CLoRA strikes a balance between parameter-efficient learning and the expansion of the rank upper bound.

During the inference and storage processes, the low-rank matrices learned by CLoRA can be seamlessly merged into the corresponding weights in MHA and FFN blocks, thus avoiding extra costs. In MHA blocks, the inputs are projected into three spaces via different projection weights to obtain the query, key, and value matrices. When the j -th LRM of CLoRA is inserted before an MHA block, we have

$$\begin{aligned} \mathbf{X}_{q/k/v} &= (\mathbf{X}_{input}^j + \mathbf{X}_{input}^j \sum_{h=1}^p \mathbf{D}_h \mathbf{Q}_i^h \mathbf{U}_h) \mathbf{W}_{q/k/v} \\ &= \mathbf{X}_{input}^j (\mathbf{I} + \sum_{h=1}^p \mathbf{D}_h \mathbf{Q}_i^h \mathbf{U}_h) \mathbf{W}_{q/k/v}, \end{aligned} \quad (16)$$

where $\mathbf{X}_{q/k/v}$ is the acquired query/key/value matrix and $\mathbf{W}_{q/k/v}$ denote the related projection weight. In FFN blocks, the inputs are first mapped into a high-dimensional space and then reprojected into the original space. Suppose \mathbf{W}_1 is the first projection weight and $\mathbf{X}_{FFN,1}$ is the representation in the high-dimensional space. When the j -th LRM of CLoRA is inserted before an FFN block, we have

$$\begin{aligned} \mathbf{X}_{FFN,1} &= (\mathbf{X}_{input}^j + \mathbf{X}_{input}^j \sum_{h=1}^p \mathbf{D}_h \mathbf{Q}_i^h \mathbf{U}_h) \mathbf{W}_1 \\ &= \mathbf{X}_{input}^j (\mathbf{I} + \sum_{h=1}^p \mathbf{D}_h \mathbf{Q}_i^h \mathbf{U}_h) \mathbf{W}_1. \end{aligned} \quad (17)$$

According to equations (16-17), the extra matrices introduced by CLoRA can be incorporated into the related projection weights contained in the pretrained ViT backbone. In other words, CLoRA doesn't change the structure of the original backbone by substituting $\mathbf{W}_{q/k/v}$ and \mathbf{W}_1 with $(\mathbf{I} + \sum_{h=1}^p \mathbf{D}_h \mathbf{Q}_i^h \mathbf{U}_h) \mathbf{W}_{q/k/v}$ and $(\mathbf{I} + \sum_{h=1}^p \mathbf{D}_h \mathbf{Q}_i^h \mathbf{U}_h) \mathbf{W}_1$ respectively, adding no extra computational or storage costs.

B. Sample-Agnostic Diversity Enhancement

As illustrated in equation (11), for the j -th LRM, its input representation update is captured by projection matrices $\{\mathbf{D}_h \mathbf{Q}_i^h \mathbf{U}_h\}_{h=1}^p$. The learning scheme can be regarded as a simplified form of MoE [47], where different projection matrices represent different experts. The performance of MoE is usually degraded by the redundant information among experts, and improving expert diversity is an effective way to address this issue [52], [53]. Therefore, the focus of this section is to design diverse projection matrices.

For convenience, we let $\mathbf{M}_h^j = \mathbf{D}_h \mathbf{Q}_i^h \mathbf{U}_h$ and denote \mathbf{X}_{input}^j as $(\mathbf{x}_1^j; \dots; \mathbf{x}_a^j; \dots; \mathbf{x}_{n+1}^j)$ where $\mathbf{x}_a^j \in R^{1 \times d}$ represents the a -th token. When \mathbf{x}_a^j is input into the j -th LRM, its representations obtained by these experts are $\{\mathbf{x}_a^j \mathbf{M}_h^j\}_{h=1}^p$. Much redundant information will exist in these representations

if they are highly similar. In other words, lower similarity implies higher diversity. In practice, the similarities among vectors are normally measured by cosine similarity. As for the h -th and the r -th representations, the similarity $s_{h,r}^{a,j}$ between them can be calculated as

$$s_{h,r}^{a,j} = \frac{\mathbf{x}_a^j \mathbf{M}_h^j (\mathbf{x}_a^j \mathbf{M}_r^j)^T}{\|\mathbf{x}_a^j \mathbf{M}_h^j\| \|\mathbf{x}_a^j \mathbf{M}_r^j\|} = \frac{\mathbf{x}_a^j \mathbf{M}_h^j (\mathbf{M}_r^j)^T (\mathbf{x}_a^j)^T}{\|\mathbf{x}_a^j \mathbf{M}_h^j\| \|\mathbf{x}_a^j \mathbf{M}_r^j\|}, \quad (18)$$

where $(\cdot)^T$ denote the transpose operator and $|\cdot|$ represent the magnitude of a vector.

When the batch size is 1, the diversity of projection matrices $\{\mathbf{D}_h \mathbf{Q}_h^j \mathbf{U}_h\}_{h=1}^p$ can be naturally enhanced by minimizing the similarity regularization term SR^j as follows.

$$SR^j = \sum_{a=1}^{n+1} \sum_{h=1}^p \sum_{r=h+1}^p (s_{h,r}^{a,j})^2. \quad (19)$$

When calculating SR^j , the main computational complexity is $\mathcal{O}((p^2n + p^2 + pn + p)d^2)$. Since this term is sample-dependent, the total computational complexity caused by a LRM is $\mathcal{O}((p^2n + p^2 + pn + p)bd^2)$, where b represents the batch size in the training process. Clearly, computing the similarity regularization term becomes computationally expensive as b increases.

Observing equation (18), we find that $\mathbf{M}_h^j (\mathbf{M}_r^j)^T$ is the dominant factor affecting the final similarity and $\mathbf{M}_h^j (\mathbf{M}_r^j)^T \rightarrow \mathbf{0}$ indicates $s_{h,r}^{a,j} \rightarrow 0$. Based on these observations, we propose a sample-agnostic diversity enhancement (SADE) scheme to reduce the high computational complexity induced by sample-dependent similarity. In SADE, we just focus on minimizing the distance between $\mathbf{M}_h^j (\mathbf{M}_r^j)^T$ and $\mathbf{0}$, without considering any token contained in \mathbf{X}^{input} and any input samples. Following equation (19), we give the reformulated similarity-regularized (RSR) term as follows.

$$RSR^j = \sum_{h=1}^p \sum_{r=h+1}^p \left\| \mathbf{M}_h^j (\mathbf{M}_r^j)^T \right\|_F^2, \quad (20)$$

where $\|\cdot\|_F^2$ represents the squared Frobenius norm.

According to equation (20), the proposed SADE scheme needs about $\mathcal{O}((0.5p^2 + 0.5p)d^3)$. When $b > \frac{d}{2(n+1)}$, $(p^2n + p^2 + pn + p)bd^2 > (0.5p^2 + 0.5p)d^3$, meaning that SADE is more computationally efficient than the sample-dependent similarity presented in equation (19). In ViT backbones, $\frac{d}{2(n+1)}$ is small enough. Taking the widely used ViT-Base, ViT-Large, and ViT-Huge backbones in [1] as examples, we report the reduced computational complexity of SADE in terms of GFLOPs in TABLE I, compared to the sample-dependent similarity.

TABLE I
REDUCED GFLOPS ACHIEVED BY SADE FOR VARYING b .

Backbone	$\frac{d}{2(n+1)}$	$b = 2$	$b = 4$	$b = 8$	$b = 16$	$b = 32$	$b = 64$
ViT-Base	1.95	↓2.5%	↓51.3%	↓75.6%	↓87.8%	↓93.9%	↓97.0%
ViT-Large	2.60	-	↓35.0%	↓67.5%	↓83.8%	↓91.9%	↓95.9%
ViT-Huge	3.25	-	↓18.8%	↓59.4%	↓79.7%	↓89.9%	↓94.9%

C. Objective Function

To expand the rank upper bound and keep the parameter-efficient property, all down/up-projection weights of inserted LRMs share the same base down/up-projection matrices in CLoRA. The additional parameters brought by base-space sharing are trained with the original loss function of each downstream task, without introducing any extra loss term. In SADE, we introduce the similarity regularization term shown in equation (20) to improve the quality of the learned input representation updates. This term is optimized as part of the final loss function. Therefore, the final objective function is written as

$$o = loss_{original} + \frac{\alpha}{d^2} \sum_{j=1}^{2L} RSR^j, \quad (21)$$

where α is a balance parameter; $loss_{original}$ represents the loss of the related downstream task. For example, $loss_{original}$ can be the average cross-entropy loss over training samples for classification tasks.

D. Comparison to Existing Work

Some learning strategies of CLoRA share similarities with those in ARC [17] and PEGO [19]. For instance, similar to ARC, the LRMs in CLoRA are designed to learn the input representation updates of MHA and FFN blocks; the LRMs in both CLoRA and PEGO contain multiple down-projection and up-projection matrices. However, CLoRA is substantially different from the two methods. The key differences are summarized as follows.

In ARC, the LRMs for MHA (or FFN) blocks share the same symmetric down-projections and up-projections. Note that the projections applied in the two types of blocks are different. Additionally, low-dimensional re-scaling coefficients for LRMs are used to obtain block-specific representations. Although the parameter-sharing strategy in ARC can compress the number of new parameters, the symmetry constraint limits the learning directions of projection matrices. In PEGO, the LRMs generate the final projection matrices by combining multiple independent low-rank matrices, leading to a significant increase in the number of trainable parameters. Suppose \mathbf{G}_f and \mathbf{G}_v are the f -th and the v -th projection matrices generated in the j -th LRMs. PEGO enhances the diversity between the two projection matrices by encouraging $(\mathbf{G}_f)^T \mathbf{G}_v$ to approximate $\mathbf{0}$.

Following a learning scheme similar to that of LoRA, ARC learns the projection matrix $\Delta \mathbf{W}_j$ in the j -th LRM using low-rank matrix $\mathbf{A}_j \mathbf{B}_j$. However, high performance is often accompanied by a large rank upper bound, which leads to an excessive number of trainable parameters. Unlike ARC, CLoRA learns $\Delta \mathbf{W}_j$ through utilizing the information existing in $\{\mathbf{A}_i \mathbf{B}_i\}_{i=1}^m$. In addition, CLoRA significantly reduces the number of trainable parameters by the base-space sharing component. After incorporating $\{\mathbf{A}_i \mathbf{B}_i\}_{i=1}^m$ into all tuning modules, each LRM in CLoRA consists of a set of low-rank projection matrices. The LRMs in PEGO are trained independently, whereas in CLoRA they are jointly trained from the shared down/up-projection spaces. Similar to PEGO, CLoRA

adopts the SADE component to improve the diversity of the learned information in each LRM. But the adopted diversity-induced strategies in PEGO and CLoRA are fundamentally different. For simplicity, we also use the above generated projection matrices \mathbf{G}_f and \mathbf{G}_v to exemplify the strategy of SADE. Under this strategy, we expect to minimize the distance between $\mathbf{G}_f(\mathbf{G}_v)^T$ and $\mathbf{0}$ to decrease the similarity between the representations extracted by \mathbf{G}_f and \mathbf{G}_v . However, PEGO just focuses on the orthogonality between the columns of \mathbf{G}_f and \mathbf{G}_v .

V. EXPERIMENTS

Extensive experiments are carried out to validate the learning performance of our proposed method in this section. Since ViT is originally designed for visual classification tasks, existing studies [17], [21], [38], [39] typically evaluate their methods on VTAB-1K benchmark [54] and fine-grained visual classification (FGVC) benchmark [12]. For fair comparisons, we also evaluate CLoRA on the two benchmarks. As introduced in Section IV, CLoRA includes base-space sharing and SADE components. Ablation studies are conducted to further analyze our proposed method. Unless otherwise specified, we use the ViT-B/16 backbone [1] pre-trained on ImageNet-21K dataset for 2D visual tasks. Recently, ViT has been extended to the field of point cloud analysis. Since the network structures of these extensions are similar to the original ViT, CLoRA can be directly incorporated into their pre-trained backbones. Following IDPT [55], DAPT [41] and PointGST [56], we also test CLoRA’s fine-tuning performance on the tasks of point cloud object recognition and part segmentation. For comparison methods, we directly adopt their reported results when available; otherwise, we run their released code following the parameter settings provided in the original papers.

A. Experiments on the VTAB-1K Benchmark

VTAB-1K is composed of 19 visual classification datasets which are categorized into three groups: **Natural** (containing 7 datasets), **Specialized** (containing 4 datasets) and **Structured** (containing 8 datasets). More details are provided in TABLE. II, where “#Class”, “#Training”, “#Validation” and “#Test” represent the number of classes, training samples, validation samples and test samples, respectively. We follow the same standard data augmentations as described in VPT [12] to maintain consistency.

Fully fine-tuning the whole pre-trained backbone (denoted as Full) and tuning the linear prediction head only (denoted as Linear) are two traditional fine-tuning methods. Here, we compare CLoRA with the two traditional fine-tuning methods and competitive PEFT baselines. The selected PEFT methods are LoRA [13], VPT [12], ARC [17], NOAH [42], RLRR [39], SCT [40], SA2VP [21], DoRA [14], PEGO [19], LoRA+AOFT [45] and CDRA-SPT [38]. In TABLE. III, we give the parameter settings of CLoRA. Following VPT, we first adopt the training (800)-validation (200) data split to determine the suitable parameter settings, then conduct tuning experiments on the entire 1000 training data using these

TABLE II
DETAILS OF THE VTAB-1K BENCHMARK.

Dataset	Group	#Class	#Training	#Validation	#Test
Cifar100		100			10000
Caltech101		102			6084
DTD		47			1880
Flower102	Natural	102	800/1000	200	6149
Pets		37			3669
SVHN		10			26032
Sun397		397			21750
Camelyon		2			32768
EuroSAT	Specialized	10	800/1000	200	5400
Resisc45		45			6300
Retinopathy		5			42670
Clevr-Count		8			15000
Clevr-Dist		6			15000
DMLab		6			22735
KITTI-Dist	Structured	4	800/1000	200	711
dSpr-Loc		16			73728
dSpr-Ori		16			73728
sNORB-Azim		18			12150
sNORB-Ele		9			12150

TABLE III
PARAMETER SETTINGS OF CLoRA ON 2D VISUAL TASKS.

Name	Value
Optimizer	Adam
Learning Rate	{0.03,0.01,0.005,0.003,0.001}
Weight Decay	{0.05,0.01,0.005,0.001}
Batch Size	32
Learning Rate Schedule	Cosine Decay
Warmup Epochs	10
Training Epochs	100
α	{0.1,1.0,10.0}
p	{4,6,8,10}
r	8

settings and finally report the top-1 test accuracy on each dataset.

The comparison results on the VTAB-1K benchmark are reported in TABLE. IV. From these experimental results, we have the following observations. 1) PEFT methods have obvious advantages over full fine-tuning (Full) and linear probing (Linear). Although full fine-tuning introduces a large number of trainable parameters, it tends to be negatively affected by overfitting due to the lack of sufficient training data. Linear probing reduces the number of trainable parameters by only tuning the linear prediction head, but it cannot obtain task-specific representations. These drawbacks explain why both linear probing and full fine-tuning obtain the worst and the second-worst mean results. 2) CLoRA achieves much more competitive classification results than all comparison methods. Specifically, it exceeds the two second-best methods (RLRR and CDRA-SPT) by 0.6% in terms of mean accuracy while further reducing the number of trainable parameters by 66.67% and 77.55%, respectively. Moreover, CLoRA obtains either the highest or second-highest accuracy on 16 out of 19 datasets. 3) LoRA+AOFT and CLoRA have the smallest and the second-

TABLE IV

EXPERIMENTAL RESULTS ON THE VTAB-1K BENCHMARK. “MEAN” REPRESENTS THE AVERAGE ACCURACY OF THE 19 DATASETS. “PARAM. (M)” DENOTES THE NUMBER OF TRAINABLE PARAMETERS IN MILLIONS AND “#PARAM. (M)” MEANS THE AVERAGE PARAM. (M). “GFLOPS” REPRESENTS THE AVERAGE GFLOPS ACROSS ALL DATASETS. IN PARAMETER-EFFICIENT TUNING METHODS, **BOLD** FONT AND UNDERLINE DENOTE THE **BEST** AND THE SECOND-BEST RESULTS.

Method	Natural						Specialized			Structured									Mean(%)	#Param. (M)	
	Cifar100	Caltech101	DTD	Flower102	Pets	SVHN	Sun397	Camelyon	EuroSAT	Resisc45	Retinopathy	Clevr-Count	Clevr-Dist	DMLab	KITTI-Dist	dSpr-Loc	dSpr-Ori	SNORB-Azim	SNORB-Ele		
<i>Traditional fine-tuning methods</i>																					
Full	68.9	87.7	64.3	97.2	86.9	87.4	38.8	79.7	95.7	84.2	73.9	56.3	58.6	41.7	65.5	57.5	46.7	25.7	29.1	65.6	85.8
Linear	63.4	85.0	63.2	97.0	86.3	36.6	51.0	78.5	87.5	68.6	74.0	34.3	30.6	33.2	55.4	12.5	20.0	9.6	19.2	52.9	0.04
<i>Parameter-efficient tuning methods</i>																					
LoRA [13]	67.1	91.4	69.4	98.8	90.4	85.3	54.0	84.9	95.3	84.4	73.6	82.9	69.2	49.8	78.5	75.7	47.1	31.0	44.0	72.3	0.33
VPT [12]	78.8	90.8	65.8	98.0	88.3	78.1	49.6	81.8	<u>96.1</u>	83.4	68.4	68.5	60.0	46.5	72.8	73.6	47.9	32.9	37.8	69.4	0.60
ARC [17]	72.2	90.1	72.7	99.0	91.0	91.9	54.4	84.9	95.7	86.7	75.8	80.7	67.1	48.7	81.6	79.2	51.0	31.4	39.9	73.4	0.13
NOAH [42]	69.6	92.7	70.2	99.1	90.4	86.1	53.7	84.4	95.4	83.9	75.8	82.8	<u>68.9</u>	49.9	81.7	81.8	48.3	32.8	44.2	73.3	0.50
RLRR [39]	75.6	92.4	72.9	<u>99.3</u>	91.5	89.8	<u>57.0</u>	86.8	95.2	85.3	75.9	79.7	64.2	53.9	82.1	83.9	53.7	33.4	43.6	<u>74.5</u>	0.33
SCT [40]	75.3	91.6	72.2	99.2	91.1	91.2	55.0	85.0	<u>96.1</u>	86.3	<u>76.2</u>	81.5	65.1	51.7	80.2	75.4	46.2	33.2	45.7	73.6	0.15
SA2VP [21]	73.0	91.9	70.5	99.1	90.8	84.7	56.8	86.0	95.9	85.8	75.2	76.6	61.8	50.8	79.9	<u>84.5</u>	52.8	34.7	<u>45.3</u>	73.5	0.48
DoRA [14]	66.1	93.1	68.8	97.0	89.9	87.2	56.4	83.1	94.5	80.8	75.2	79.1	62.1	48.0	80.6	83.1	51.8	33.2	44.0	72.3	0.19
PEGO [19]	75.1	92.9	<u>73.1</u>	99.4	<u>92.1</u>	89.2	56.5	<u>87.0</u>	96.2	86.1	76.1	78.4	62.4	52.7	79.5	80.6	52.3	31.9	37.7	73.6	0.44
LoRA+AOFT [45]	73.6	92.6	71.1	<u>99.3</u>	91.3	85.3	56.9	84.7	94.8	83.7	75.6	76.7	63.2	48.7	81.0	82.2	<u>53.1</u>	26.9	45.1	72.9	0.08
CDRA-SPT [38]	73.8	<u>93.3</u>	72.7	99.4	91.6	89.9	55.8	86.8	96.2	86.2	76.0	83.0	<u>68.9</u>	51.5	82.1	80.9	51.7	33.0	43.2	<u>74.5</u>	0.49
CLoRA	76.3	93.8	73.4	99.4	92.4	91.3	57.8	87.4	96.2	86.4	76.4	81.6	67.3	52.9	81.9	84.7	53.7	<u>33.9</u>	40.1	75.1	0.11

smallest numbers of trainable parameters. However, compared with LoRA+AOFT, CLoRA achieves a 2.2% improvement in terms of mean accuracy. Note that CLoRA, ARC, RLRR, DoRA, PEGO and LoRA+AOFT are LoRA-based methods. CLoRA clearly performs better than LoRA and its variations (excluding LoRA+AOFT) in terms of both mean accuracy and parameter efficiency.

B. Experiments on the FGVC Benchmark

FGVC benchmark consists of five fine-grained visual classification datasets including CUB-200-2011, NABirds, Oxford Flowers, Stanford Dogs and Stanford Cars. TABLE. V shows the details of these datasets. Since the effectiveness of LoRA, VPT, ARC, RLRR, SA2VP, LoRA+AOFT and CDRA-SPT has been verified on the five datasets, they are selected as comparison methods. For the purpose of comparison, samples from the datasets are processed by the same data augmentations used in VPT.

TABLE V
DETAILS OF THE FGVC BENCHMARK.

Dataset	#Class	#Training	#Validation	#Test
CUB-200-2011 (CUB)	200	5394	600	5794
NABirds (NBirds)	555	21536	2393	24633
Oxford Flowers (Flowers)	102	1020	1020	6149
Stanford Dogs (Dogs)	120	10800	1200	8580
Stanford Cars (Cars)	196	7329	815	8041

We present the experimental results of comparison methods and CLoRA in TABLE. VI. CLoRA outperforms the second-best method (RLRR) by 0.4% in terms of mean accuracy while

TABLE VI
EXPERIMENTAL RESULTS ON THE FGVC BENCHMARK.

Method	CUB	NBirds	Flowers	Dogs	Cars	Mean(%)	Param.(M)
<i>Traditional fine-tuning methods</i>							
Full	87.3	82.7	98.8	89.4	<u>84.5</u>	88.5	85.98
Linear	85.3	75.9	97.9	86.2	51.3	79.3	0.18
<i>Parameter-efficient tuning methods</i>							
LoRA	88.3	85.6	99.2	91.0	83.2	89.5	0.44
VPT	88.5	84.2	99.0	90.2	83.6	89.1	0.85
ARC	88.5	85.3	99.3	91.9	85.7	90.1	<u>0.25</u>
RLRR	89.3	84.7	99.5	92.0	87.0	90.4	0.47
SA2VP	89.1	85.8	99.3	92.1	84.1	90.1	0.85
LoRA+AOFT	88.8	84.2	<u>99.4</u>	<u>92.0</u>	85.1	89.9	0.22
CDRA-SPT	88.6	83.4	99.3	89.8	88.2	89.9	0.74
CLoRA	89.2	85.7	99.5	92.1	<u>87.3</u>	90.8	0.25

reducing the number of trainable parameters by 46.81%. In addition, CLoRA achieves the highest classification accuracies on Flowers and Dogs datasets and obtains the second-best classification accuracies on the other datasets.

C. Experiments on Larger-Scale ViT Backbones

We further validate the performance of CLoRA on larger-scale ViT backbones. LoRA, VPT, ARC, RLRR, and LoRA+AOFT have been extensively validated on ViT-Large and ViT-Huge backbones, showing strong performance on the VTAB-1K benchmark. For comparison consistency, we also conduct experiments on the same benchmark with the two larger ViT backbones. Comparison results on ViT-Large and ViT-Huge backbones are reported in TABLE. VII and

TABLE. VIII. From the experimental results, we observe that CLoRA achieves much more competitive classification performance than the comparison methods and simultaneously introduces the smallest number of trainable parameters.

TABLE VII
COMPARISON RESULTS ON THE ViT-LARGE BACKBONE.

Method	Natural(7)	Specialized(4)	Structured(8)	Mean(%)	#Param.(M)
<i>Traditional fine-tuning methods</i>					
Full	74.7	83.8	48.1	65.4	303.40
Linear	70.9	69.1	25.8	51.5	0.05
<i>Parameter-efficient tuning methods</i>					
LoRA	70.5	85.0	57.3	72.0	0.74
VPT	82.5	83.9	54.1	70.8	0.49
ARC	82.3	85.6	57.3	72.5	0.18
RLRR	<u>83.9</u>	<u>86.4</u>	61.9	<u>75.2</u>	0.82
LoRA+AOFT	83.3	85.9	60.2	74.3	0.15
CLoRA	84.7	86.6	<u>61.5</u>	75.3	0.15

TABLE VIII
COMPARISON RESULTS ON THE ViT-HUGE BACKBONE.

Method	Natural(7)	Specialized(4)	Structured(8)	Mean(%)	#Param.(M)
<i>Traditional fine-tuning methods</i>					
Full	70.9	83.6	46.0	63.1	630.90
Linear	67.9	79.0	26.1	52.7	0.06
<i>Parameter-efficient tuning methods</i>					
LoRA	77.1	83.5	55.4	69.3	1.21
VPT	77.9	83.3	52.2	68.2	0.96
ARC	79.1	84.8	53.7	69.9	0.22
RLRR	<u>79.4</u>	<u>85.1</u>	59.0	<u>72.0</u>	1.33
LoRA+AOFT	78.8	83.8	58.3	71.3	<u>0.20</u>
CLoRA	80.7	85.6	<u>58.4</u>	72.3	0.19

D. Ablation Studies

CLoRA includes base-space sharing and SADE components. In base-space sharing, two LRM s are inserted before the MHA and FFN blocks in each encoder layer, and all down/up-projection weights in LRMs share the same down/up-projection spaces. To improve the diversity of the information learned from the shared spaces, SADE is introduced in the training process. Here, taking the VTAB-1K benchmark as an example, we first conduct ablation experiments to investigate the influence of different parts and then verify the effectiveness of base-space sharing and SADE components.

The results of ablation experiments are reported in TABLE. IX. Note that notations are listed in the first column for convenience. “✓” means the corresponding item is selected, while “✗” indicates it is not selected. For instance, in CLoRAMF, two LRMs are inserted before MHA and FFN blocks while SADE is not applied. According to the results, we observe that CLoRA exceeds CLoRAMF, CLoRAMS and CLoRAFS by 1.7%, 2.8% and 2.6%, respectively. This observation implies that adapting the input representations of FFN blocks is more important than the others and SADE has the least influence.

TABLE IX
ABLATION EXPERIMENTS ON THE VTAB-1K BENCHMARK.

Notation	Inserted Before MHA	Inserted Before FFN	SADE	Mean(%)
CLoRAMF	✓	✓	✗	73.4
CLoRAMS	✓	✗	✓	72.3
CLoRAFS	✗	✓	✓	72.5
CLoRA	✓	✓	✓	75.1

Based on LoRA, each LRM in PEGO combines a group of low-rank projection matrices which are regularized by column orthogonality. LRMs in LoRA and its variants including PEGO are usually adopted to update the query and value projection weights. Following an information-learning scheme similar to LoRA, CLoRA can be easily applied to learn the query and value weight updates by replacing the identity matrices with the corresponding projection weights. Directly calculating the similarities among the representations extracted by multiple projection matrices is computationally expensive for relatively large batch sizes. In contrast, SADE can efficiently approximate these relationships. Here, we further evaluate the performance of the two components designed for CLoRA.

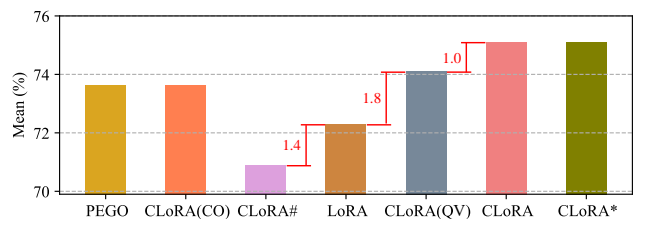


Fig. 3. Performance verification of the two components in CLoRA.

The comparison results on the VTAB-1K benchmark in terms of mean accuracy are shown in Fig. 3. CLoRA(QV) denotes the variant where LRMs are employed to learn the query and value weight updates. CLoRA(CO) replaces the SADE component with the column orthogonality regularization used in PEGO. Additionally, CLoRA(CO) follows the learning scheme provided by PEGO. By comparing PEGO, CLoRA(CO), CLoRA(QV) and LoRA, we observe that: 1) CLoRA(CO) achieves similar performance to PEGO; 2) CLoRA(QV) evidently outperforms PEGO, CLoRA(CO) and LoRA. These comparisons illustrate the effectiveness of the base-space sharing and SADE components. From the results of CLoRA (QV) and CLoRA, we observe that inserting LRMs to tune the input representations for MHA and FFN blocks enables learning more informative representations than those learned through the query and value weight updates. CLoRA# represents that the final low-rank matrices obtained by LRMs are directly learned by $\{\mathbf{A}_i \mathbf{B}_i\}_{i=1}^m$ (see equation (7)). According to these results, CLoRA exceeds CLoRA# by 4.2% and CLoRA# even underperforms LoRA, which illustrates that our designed base-space sharing component can address the potential optimization conflicts effectively. CLoRA* means that the similarities are directly calculated using equation (18). Compared with CLoRA*, CLoRA performs comparably while achieving a 93.9% reduction in GFLOPs (see TABLE. I),

TABLE X

CLASSIFICATION ACCURACY (%) ON MODELNET40 DATASET AND THREE VARIANTS OF SCANOBJECTNN DATASET. #PARAM. (M) AND #GFLOPS DENOTE THE AVERAGE NUMBER OF TRAINABLE PARAMETERS AND THE AVERAGE GFLOPS ACROSS ALL DATASETS.

Pre-trained model	Fine-tuning strategy	Reference	#Param. (M)	#GFLOPs	ScanObjectNN			ModelNet40
					OBJ_BG	OBJ_ONLY	PB_T50_RS	
Point-MAE [61]	Full	-	22.1 (100%)	4.76	90.02	88.29	85.18	93.2
	IDPT [55]	ICCV 23	1.7 (7.69%)	7.10(↑)	91.22(+1.20)	90.02(+1.73)	84.94(-0.24)	93.3(-0.1)
	Point-PEFT [63]	AAAI 24	0.7 (3.13%)	7.61(↑)	89.67(-0.35)	88.98(+0.69)	84.91(-0.27)	93.3(+0.1)
	DAPT [41]	CVPR 24	1.1 (4.97%)	4.96(↑)	90.88(+0.86)	90.19(+1.90)	85.08(-0.10)	93.5(+0.3)
	PointGST [56]	TPAMI 25	0.6 (2.77%)	4.81(↑)	91.74(+1.72)	90.19(+1.90)	85.29(+0.11)	93.5(+0.3)
	PointLoRA [64]	CVPR 25	0.8 (3.43%)	5.06(↑)	90.71(+0.69)	89.33(+1.04)	85.53(+0.35)	93.3(+0.1)
Point-BERT [60]	CLoRA(ours)	-	0.3 (1.36%)	4.76(-)	91.57(+1.55)	90.19(+1.90)	85.32(+0.14)	93.6(+0.4)
	Full	-	22.1 (100%)	4.76	87.43	88.12	83.07	92.7
	IDPT [55]	ICCV 23	1.7 (7.69%)	7.10(↑)	88.12(+0.69)	88.30(+0.18)	83.69(+0.62)	92.6(-0.1)
	Point-PEFT [63]	AAAI 24	0.7 (3.13%)	7.61(↑)	88.81(+1.38)	89.67(+1.55)	85.00(+1.93)	93.4(+0.7)
	DAPT [41]	CVPR 24	1.1 (4.97%)	4.96(↑)	91.05(+3.62)	89.67(+1.55)	85.43(+2.36)	93.1(+0.4)
	PointGST [56]	TPAMI 25	0.6 (2.77%)	4.81(↑)	91.39(+3.96)	89.67(+1.55)	85.64(+2.57)	93.4(+0.7)
RECON [62]	PointLoRA [64]	CVPR 25	0.9 (4.07%)	5.06(↑)	89.85(+2.42)	88.98(+0.86)	84.63(+1.56)	93.2(+0.5)
	CLoRA(ours)	-	0.3 (1.36%)	4.76(-)	91.74(+4.31)	90.36(+2.24)	85.80(+2.73)	93.4(+0.7)
	Full	-	22.1 (100%)	4.76	94.32	92.77	90.01	92.5
	IDPT [55]	ICCV 23	1.7 (7.69%)	7.10(↑)	93.29(-1.03)	91.57(-1.20)	87.27(-2.74)	93.4(+0.9)
	Point-PEFT [63]	AAAI 24	0.7 (3.13%)	7.61(↑)	91.91(-2.41)	90.19(-2.58)	86.36(-3.65)	93.3(+0.8)
	DAPT [41]	CVPR 24	1.1 (4.97%)	4.96(↑)	94.32(+0.00)	92.43(-0.34)	89.38(-0.63)	93.5(+1.0)

indicating the efficiency brought by SADE.

TABLE XI
PARAMETER SETTINGS OF CLoRA ON POINT CLOUD DATASETS.

Name	Value
Number of Points	1024 (ModelNet40) 2048 (ScanObjectNN&ShapeNetPart)
Batch Size	32 (ModelNet40&ScanObjectNN) 16 (ShapeNetPart)
Learning Rate	0.0005 (ModelNet40&ScanObjectNN) 0.0002 (ShapeNetPart)
Weight Decay	0.05
Optimizer	AdamW
Learning Rate Schedule	Cosine Decay
Warmup Epochs	10
Training Epochs	300
α	{0.01,0.1,1.0,10.0}
p	{6,8,10,12}
r	8

E. Further Exploration

Since pre-trained point cloud transformers share similar encoder blocks with ViT, CLoRA can be directly applied to adapt these models for downstream tasks. Consistent with related methods [41], [55], we verify the performance of CLoRA on three widely used point cloud datasets: ModelNet40 [57], ScanObjectNN [58] and ShapeNetPart [59]. Both ModelNet40 and ScanObjectNN are point cloud object recognition datasets. ModelNet40 consists of 12311 CAD models from 40 classes. All point clouds in ModelNet40

are complete, uniform and noise-free. Besides, they are independently and identically distributed. ScanObjectNN contains approximately 15000 real-world point cloud instances covering 15 indoor object categories. It includes three variants (OBJ_BG, OBJ_ONLY, PB_T50_RS) arranged in order of increasing difficulty. ShapeNetPart is a widely used dataset for point-level part segmentation and it comprises 16881 samples across 16 object types and 50 part categories.

Following IDPT [55] and DAPT [41], we select Point-BERT [60], Point-MAE [61], and RECON [62] as pre-trained backbones. IDPT, Point-PEFT [63], DAPT, PointGST [56] and PointLoRA [64] are excellent PEFT methods for point cloud learning and are therefore selected as comparison methods in this subsection. Additionally, full fine-tuning (Full) serves as the baseline. For fair comparisons, we adopt the same data augmentation techniques used in [41]. Note that all experimental results are reported without voting strategies.

1) Experiments on Point Cloud Object Recognition

The classification results of the comparison methods and CLoRA are presented in TABLE. X. Based on IDPT and DAPT, the parameter settings of CLoRA used in these experiments are provided in TABLE. XI. All methods are compared using three metrics: 1) the average number of trainable parameters (#Param.(M)); 2) the average GFLOPs (#GFLOPs); and 3) top-1 classification accuracy. Observing these results, we find that CLoRA achieves the highest or the second-highest classification accuracy across different pre-trained backbones and datasets. Among the comparison methods, PointGST introduces the fewest trainable parameters when fine-tuning Point-BERT, Point-MAE and RECON backbones. Nevertheless, compared with PointGST, CLoRA further re-

duces the parameter count by 50%, 50%, and 33.3%, respectively, demonstrating its strong parameter efficiency. Although IDPT, Point-PEFT, DAPT, PointGST and PointLoRA perform well in terms of classification accuracy and the number of trainable parameters, they bring extra computational cost at the inference stage. In contrast, the trainable modules designed for CLoRA can be seamlessly incorporated into the original backbones at the inference stage, without introducing extra cost.

We further evaluate the few-shot learning ability of our proposed method by conducting few-shot experiments on the ModelNet40 dataset. Following the same data settings provided by Zha et al. [54], we report the learning results in TABLE. XII. In low-data scenarios, CLoRA achieves the highest accuracy in most cases across the three backbones when compared to IDPT, Point-PEFT, DAPT, and PointLoRA. While PointGST performs better than CLoRA on the Point-MAE backbone, CLoRA outperforms PointGST on the RECON backbone. These results demonstrate the effectiveness of CLoRA under low-data regimes.

TABLE XII
FEW-SHOT LEARNING RESULTS ON THE MODELNET40 DATASET.
RESULTS ARE PRESENTED AS MEAN CLASSIFICATION ACCURACY
(%) \pm STANDARD DEVIATION (%) OVER 10 INDEPENDENT EXPERIMENTS.

Method	Reference	5-way		10-way	
		10-shot	20-shot	10-shot	20-shot
<i>Pre-trained Point-MAE backbone</i>					
+ Full	ECCV 22	96.3 \pm 2.5	97.8 \pm 1.8	92.6 \pm 4.1	95.0 \pm 3.0
+ IDPT	ICCV 23	97.3 \pm 2.1	97.9 \pm 1.1	92.8 \pm 4.1	95.4 \pm 2.9
+ Point-PEFT	AAAI 24	95.5 \pm 2.9	97.6 \pm 1.7	91.7 \pm 4.3	94.7 \pm 3.0
+ DAPT	CVPR 24	96.8 \pm 1.8	98.0 \pm 1.0	93.0 \pm 3.5	95.5 \pm 3.2
+ PointGST	TPAMI 25	98.0 \pm 1.8	98.3 \pm 0.9	93.7 \pm 4.0	95.7 \pm 2.4
+ PointLoRA	CVPR 25	96.6 \pm 2.6	97.7 \pm 1.3	92.0 \pm 4.2	95.2 \pm 3.3
+ CLoRA	-	96.8 \pm 1.9	98.1 \pm 1.1	92.2 \pm 4.1	95.6 \pm 2.9
<i>Pre-trained Point-BERT backbone</i>					
+ Full	CVPR 22	94.6 \pm 3.1	96.3 \pm 2.7	91.0 \pm 5.4	92.7 \pm 5.1
+ IDPT	ICCV 23	96.0 \pm 1.7	97.2 \pm 2.6	91.9 \pm 4.4	93.6 \pm 3.5
+ Point-PEFT	AAAI 24	95.4 \pm 3.0	97.3 \pm 1.9	91.6 \pm 4.5	94.5 \pm 3.5
+ DAPT	CVPR 24	95.8 \pm 2.1	97.3 \pm 1.3	92.2 \pm 4.3	94.2 \pm 3.4
+ PointGST	TPAMI 25	96.5 \pm 2.4	97.9 \pm 2.0	92.7 \pm 4.2	95.0 \pm 2.8
+ PointLoRA	CVPR 25	95.7 \pm 2.5	97.8 \pm 1.7	92.0 \pm 4.1	94.7 \pm 3.0
+ CLoRA	-	96.1 \pm 2.3	98.0 \pm 1.7	92.4 \pm 4.0	95.1 \pm 2.7
<i>Pre-trained RECON backbone</i>					
+ Full	ICML 23	93.7 \pm 1.9	98.9 \pm 1.2	93.3 \pm 3.9	95.8 \pm 3.0
+ IDPT	ICCV 23	96.0 \pm 1.7	97.2 \pm 2.6	91.9 \pm 4.4	93.6 \pm 3.5
+ Point-PEFT	AAAI 24	95.4 \pm 3.0	97.3 \pm 1.9	91.6 \pm 4.5	94.5 \pm 3.5
+ DAPT	CVPR 24	95.8 \pm 2.1	97.3 \pm 1.3	92.2 \pm 4.3	94.2 \pm 3.4
+ PointGST	TPAMI 25	96.5 \pm 2.4	97.9 \pm 2.0	92.7 \pm 4.2	95.0 \pm 2.8
+ PointLoRA	CVPR 25	96.9 \pm 2.7	98.8 \pm 1.2	92.7 \pm 4.4	95.8 \pm 2.9
+ CLoRA	-	96.7 \pm 2.1	98.2 \pm 1.5	92.8 \pm 4.1	95.7 \pm 3.0

2) Experiments on Point Cloud Part Segmentation

TABLE XIII presents the part segmentation results on the ShapeNetPart dataset, following the parameter settings provided in TABLE XI. Full fine-tuning almost outperforms all PEFT methods including CLoRA. However, it requires a large number of trainable parameters, which is inefficient for adapting pre-trained backbones to downstream tasks and imposes significant storage overhead. Therefore, we focus

on comparing the learning performance of PEFT methods. According to the experimental results, CLoRA achieves comparable or superior performance compared to the best among IDPT, Point-PEFT, DAPT, PointGST, and PointLoRA. More importantly, CLoRA has an obvious advantage in reducing the number of trainable parameters.

TABLE XIII

PART SEGMENTATION RESULTS ON THE SHAPENETPART DATASET. CLS. MIOU (%) AND INST. MIOU (%) REPRESENT THE CLASS-AVERAGED AND INSTANCE-AVERAGED MIOU, RESPECTIVELY.

Method	Reference	Params. (M)	Cls. mIoU (%)	Inst. mIoU (%)
<i>Pre-trained Point-MAE backbone</i>				
+ Full	ECCV 22	27.06	84.19	86.1
+ IDPT	ICCV 23	5.69	83.79	85.7
+ Point-PEFT	AAAI 24	5.62	83.20	85.2
+ DAPT	CVPR 24	5.65	84.01	85.7
+ PointGST	TPAMI 25	5.59	83.81	85.8
+ PointLoRA	CVPR 25	5.71	83.74	85.3
+ CLoRA	-	5.29	84.03	85.7
<i>Pre-trained Point-BERT backbone</i>				
+ Full	CVPR 22	27.06	84.11	85.6
+ IDPT	ICCV 23	5.69	83.50	85.3
+ Point-PEFT	AAAI 24	5.62	81.12	84.3
+ DAPT	CVPR 24	5.65	83.83	85.5
+ PointGST	TPAMI 25	5.58	83.87	85.7
+ PointLoRA	CVPR 25	5.68	82.61	85.2
+ CLoRA	-	5.30	83.81	85.5
<i>Pre-trained RECON backbone</i>				
+ Full	ICML 23	27.06	84.52	86.1
+ IDPT	ICCV 23	5.69	83.66	85.7
+ Point-PEFT	AAAI 24	5.62	83.10	85.1
+ DAPT	CVPR 24	5.65	83.87	85.7
+ PointGST	TPAMI 25	5.58	83.98	85.8
+ PointLoRA	CVPR 25	5.63	83.98	85.4
+ CLoRA	-	5.29	83.98	85.6

VI. CONCLUSION AND FUTURE WORK

A novel parameter-efficient fine-tuning method termed collaborative low-rank adaptation (CLoRA) is proposed in this paper. CLoRA includes two key components: base-space sharing and SADE. In base-space sharing, all LRM share the same down/up-projection spaces to increase their learning capacities and reduce the number of trainable parameters. Each LRM in CLoRA constructs multiple low-rank matrices from the shared spaces and combines the representations extracted by these matrices. To further improve the performance of LRMs, SADE is applied to regularize the relationship among the combined representations. Note that all learned low-rank matrices of CLoRA can be seamlessly incorporated into the related weights of fine-tuned backbones, without introducing extra inference and storage costs. Experimental results on image and point cloud benchmarks illustrate that CLoRA has an excellent ability to keep a balance between learning performance and parameter efficiency. Additionally, CLoRA achieves the state-of-the-art inference efficiency on point cloud benchmarks.

Similar to existing PEFT methods, CLoRA performs well on downstream tasks when provided with high-quality data.

Nevertheless, in some practical application scenarios, such as underwater target recognition and autonomous driving, the collected samples are often of low quality, posing significant challenges for effective fine-tuning. In future work, we will focus on designing suitable representation-learning strategies to extract robust task-specific representations by leveraging the knowledge contained in pre-trained models.

REFERENCES

- [1] A. Dosovitskiy, L. Beyer, A. Kolesnikov, et al, “An image is worth 16x16 words: Transformers for image recognition at scale,” in *Proceedings of the International Conference on Learning Representations (ICLR)*, 2021.
- [2] Y. Liu, Y. Zhang, Y. Wang, et al, “A survey of visual transformers,” *IEEE Transactions on Neural Networks and Learning Systems*, vol.35, no.6, pp.7478-7498, 2024.
- [3] Y. Wu, Y. Li, M. Liu, et al, “Learning an adaptive and view-invariant vision transformer for real-time UAV tracking,” *IEEE Transactions on Circuits and Systems for Video Technology*, Early Access, 2025.
- [4] J. Li, L. Yang and Q. Hu, “Enhancing multi-source open-set domain adaptation through nearest neighbor classification with self-supervised vision transformer,” *IEEE Transactions on Circuits and Systems for Video Technology*, vol.34, no.4, pp.2648-2662, 2024.
- [5] U. Evci, V. Dumoulin, H. Larochelle, et al, “Head2toe: Utilizing intermediate representations for better transfer learning,” in *Proceedings of the International Conference on Machine Learning (ICML)*, pp.6009-6033, 2022.
- [6] M. Dehghani, J. Djolonga, B. Mustafa, et al, “Scaling vision transformers to 22 billion parameters,” in *Proceedings of the International Conference on Machine Learning (ICML)*, pp.7480-7512, 2023.
- [7] C. Xia, X. Wang, F. Lv, et al, “Vit-comer: Vision transformer with convolutional multi-scale feature interaction for dense predictions,” in *Proceedings of the IEEE/CVF Conference on Computer Vision and Pattern Recognition (CVPR)*, pp.5493-5502, 2024.
- [8] Z. Liu, J. Zhu, N. Li, et al, “Multiple-Exit Tuning: Towards inference-efficient adaptation for vision transformer,” *IEEE Transactions on Circuits and Systems for Video Technology*, Early Access, 2025.
- [9] Y. Liu, Y. Li, X. Lan, et al, “UP-Person: Unified parameter-efficient transfer learning for text-based person retrieval,” *IEEE Transactions on Circuits and Systems for Video Technology*, vol.35, no.12, pp.12874-12889, 2025.
- [10] Z. Peng, Z. Xu, Z. Zeng, et al, “Parameter efficient fine-tuning via cross block orchestration for segment anything model,” in *Proceedings of the IEEE/CVF Conference on Computer Vision and Pattern Recognition (CVPR)*, pp.3743-3752, 2024.
- [11] N. Houlsby, A. Giurgiu, S. Jastrzebski, et al, “Parameter-efficient transfer learning for NLP,” in *Proceedings of the International Conference on Machine Learning (ICML)*, pp.2790-2799, 2019.
- [12] M. Jia, L. Tang, B.C. Chen, et al, “Visual prompt tuning,” in *Proceedings of the European Conference on Computer Vision (ECCV)*, pp.709-727, 2022.
- [13] E.J. Hu, Y. Shen, P. Wallis, et al, “LoRA: Low-rank adaptation of large language models,” in *Proceedings of the International Conference on Learning Representations (ICLR)*, 2022.
- [14] S. Liu, C. Wang, H. Yin, et al, “Dora: Weight-decomposed low-rank adaptation,” in *Proceedings of the International Conference on Machine Learning (ICML)*, pp.1-22, 2024.
- [15] J. Gu, J. Yuan, J. Cai, et al, “La-LoRA: Parameter-efficient fine-tuning with layer-wise adaptive low-rank adaptation,” *Neural Networks*, vol.194, 108095, 2026.
- [16] A. Agiza, M. Neseem, S. Reda, “Mtlora: Low-rank adaptation approach for efficient multi-task learning,” in *Proceedings of the IEEE/CVF Conference on Computer Vision and Pattern Recognition (CVPR)*, pp.16196-16205, 2024.
- [17] W. Dong, D. Yan, Z. Lin, et al, “Efficient adaptation of large vision transformer via adapter re-composing,” in *Proceedings of the Conference on Neural Information Processing Systems (NeurIPS)*, vol.36, pp.52548-52567, 2023.
- [18] S. Jie, H. Wang, Z. Deng, “Revisiting the parameter efficiency of adapters from the perspective of precision redundancy,” in *Proceedings of the IEEE/CVF International Conference on Computer Vision (ICCV)*, pp.17217-17226, 2023.
- [19] J. Hu, J. Zhang, L. Qi, et al, “Learn to preserve and diversify: Parameter-efficient group with orthogonal regularization for domain generalization,” in *Proceedings of the European Conference on Computer Vision (ECCV)*, pp.198-216, 2024.
- [20] Y. Wang, Z. Huang, X. Hong, “S-prompts learning with pre-trained transformers: An occam’s razor for domain incremental learning,” in *Proceedings of the Conference on Neural Information Processing Systems (NeurIPS)*, vol.35, pp.5682-5695, 2022.
- [21] W. Pei, T. Xia, F. Chen, et al, “SA2VP: Spatially aligned-and-adapted visual prompt,” in *Proceedings of the AAAI Conference on Artificial Intelligence*, vol.38, no.5, pp.4450-4458, 2024.
- [22] C. Tu, Z. Mai, W. Chao, “Visual query tuning: Towards effective usage of intermediate representations for parameter and memory efficient transfer learning,” in *Proceedings of the IEEE/CVF Conference on Computer Vision and Pattern Recognition (CVPR)*, pp.7725-7735, 2023.
- [23] T. Zhang, J. Bai, Z. Lu, et al, “Parameter-efficient and memory-efficient tuning for vision transformer: a disentangled approach,” in *Proceedings of the European Conference on Computer Vision (ECCV)*, pp.346-363, 2024.
- [24] X. Nie, B. Ni, J. Chang, et al, “Pro-tuning: Unified prompt tuning for vision tasks,” *IEEE Transactions on Circuits and Systems for Video Technology*, vol.34, no.6, pp.4653-4667, 2024.
- [25] M. Karimi, J. Henderson, S. Ruder, “Compacter: Efficient low-rank hypercomplex adapter layers,” in *Proceedings of the Conference on Neural Information Processing Systems (NeurIPS)*, vol.34, pp.1022-1035, 2021.
- [26] J. Steitz, S. Roth, “Adapters strike back,” in *Proceedings of the IEEE/CVF Conference on Computer Vision and Pattern Recognition (CVPR)*, pp.23449-23459, 2024.
- [27] S. Chen, C. Ge, Z. Tong, et al, “Adaptformer: Adapting vision transformers for scalable visual recognition,” in *Proceedings of the Conference on Neural Information Processing Systems (NeurIPS)*, vol.35, pp.16664-16678, 2022.
- [28] Y. Xin, J. Du, Q. Wang, et al, “Vmt-adapter: Parameter-efficient transfer learning for multi-task dense scene understanding,” in *Proceedings of the AAAI Conference on Artificial Intelligence*, vol.38, no.14, pp.16085-16093, 2024.
- [29] Z. Jiang, C. Mao, Z. Huang, et al, “Res-tuning: A flexible and efficient tuning paradigm via unbinding tuner from backbone,” in *Proceedings of the Conference on Neural Information Processing Systems (NeurIPS)*, vol.36, pp.42689-42716, 2023.
- [30] J. Pan, Z. Lin, X. Zhu, et al, “St-adapter: Parameter-efficient image-to-video transfer learning,” in *Proceedings of the Conference on Neural Information Processing Systems (NeurIPS)*, vol.35, pp.26462-26477, 2022.
- [31] T. Chen, L. Zhu, C. Deng, et al, “Sam-adapter: Adapting segment anything in underperformed scenes,” in *Proceedings of the IEEE/CVF International Conference on Computer Vision (ICCV)*, pp.3367-3375, 2023.
- [32] Y. Sung, J. Cho, M. Bansal, “LST: Ladder side-tuning for parameter and memory efficient transfer learning,” in *Proceedings of the Conference on Neural Information Processing Systems (NeurIPS)*, vol.35, pp.12991-13005, 2022.
- [33] D. Yin, X. Han, B. Li, et al, “Parameter-efficient is not sufficient: Exploring parameter, memory, and time efficient adapter tuning for dense predictions,” in *Proceedings of the ACM International Conference on Multimedia (ACM MM)*, pp.1398-1406, 2024.
- [34] N. Tang, M. Fu, J. Wu, “Minimal Interaction Separated Tuning: A New paradigm for visual adaptation,” in *Proceedings of the IEEE/CVF Conference on Computer Vision and Pattern Recognition (CVPR)*, pp.25208-25217, 2025.
- [35] H. Diao, B. Wan, X. Jia, et al, “Sherl: Synthesizing high accuracy and efficient memory for resource-limited transfer learning,” in *Proceedings of the European Conference on Computer Vision (ECCV)*, pp.75-95, 2024.
- [36] H. Diao, B. Wan, X. Jia, et al, “Unipt: Universal parallel tuning for transfer learning with efficient parameter and memory,” in *Proceedings of the IEEE/CVF Conference on Computer Vision and Pattern Recognition (CVPR)*, pp.28729-28740, 2024.
- [37] H. He, J. Cai, J. Zhang, et al, “Sensitivity-aware visual parameter-efficient fine-tuning,” in *Proceedings of the IEEE/CVF International Conference on Computer Vision (ICCV)*, pp.11825-11835, 2023.
- [38] T. Chen, J. Chen, B. Zhang, et al, “Sensitivity-aware efficient fine-tuning via compact dynamic-rank adaptation,” in *Proceedings of the IEEE/CVF Conference on Computer Vision and Pattern Recognition (CVPR)*, pp.9655-9664, 2025.

[39] W. Dong, X. Zhang, B. Chen, et al, "Low-rank Rescaled Vision Transformer Fine-Tuning: A residual design approach," in *Proceedings of the IEEE/CVF Conference on Computer Vision and Pattern Recognition (CVPR)*, pp.16101-16110, 2024.

[40] H.H. Zhao, P. Wang, Y. Zhao, et al, "SCT: A simple baseline for parameter-efficient fine-tuning via salient channels," *International Journal of Computer Vision*, vol.132, no.3, pp.731-749, 2024.

[41] X. Zhou, D. Liang, W. Xu, et al, "Dynamic adapter meets prompt tuning: Parameter-efficient transfer learning for point cloud analysis," in *Proceedings of the IEEE/CVF Conference on Computer Vision and Pattern Recognition (CVPR)*, pp.14707-14717, 2024.

[42] Y. Zhang, K. Zhou, Z. Liu, "Neural prompt search," *IEEE Transactions on Pattern Analysis and Machine Intelligence*, vol.47, no.7, pp.5268-5280, 2025.

[43] S. Hayou, N. Ghosh, B. Yu, "Lora+: Efficient low rank adaptation of large models," in *Proceedings of the International Conference on Machine Learning (ICML)*, pp.1-24, 2024.

[44] L. Li, C. Lin, D. Li, et al, "Efficient fine-tuning of large models via nested low-rank adaptation," in *Proceedings of the IEEE/CVF International Conference on Computer Vision (ICCV)*, pp.22252-22262, 2025.

[45] Y. Yang, H. Luo, Y. Sun, et al, "Efficient adaptation of pre-trained vision transformer underpinned by approximately orthogonal fine-tuning strategy," in *Proceedings of the IEEE/CVF International Conference on Computer Vision (ICCV)*, pp.4878-4887, 2025.

[46] G. Luo, M. Huang, Y. Zhou, et al, "Towards efficient visual adaption via structural re-parameterization," 2023, *arXiv:2302.08106*. [Online]. Available: <https://arxiv.org/abs/2302.08106>

[47] W. Cai, J. Jiang, F. Wang, et al, "A survey on mixture of experts in large language models," *IEEE Transactions on Knowledge and Data Engineering*, vol.37, no.7, pp.3896-3915, 2025.

[48] X. Wu, S. Huang, F. Wei, "Mixture of lora experts," in *Proceedings of the International Conference on Learning Representations (ICLR)*, 2024.

[49] C. Tian, Z. Shi, Z. Guo, et al, "Hydralora: An asymmetric lora architecture for efficient fine-tuning," in *Proceedings of the Conference on Neural Information Processing Systems (NeurIPS)*, vol.37, pp.9565-9584, 2024.

[50] S. Dou, Z. Zhou, Y. Liu, et al, "LoRAMoE: Alleviating world knowledge forgetting in large language models via MoE-style plugin," in *Proceedings of the Annual Meeting of the Association for Computational Linguistics (ACL)*, pp.1932-1945, 2024.

[51] Y. Mao, K. Huang, C. Guan, et al, "Dora: Enhancing parameter-efficient fine-tuning with dynamic rank distribution," in *Proceedings of the Annual Meeting of the Association for Computational Linguistics (ACL)*, pp.11662-11675, 2024.

[52] Y. Zhang, J. Cai, Z. Wu, et al, "Mixture of experts as representation learner for deep multi-view clustering," in *Proceedings of the AAAI Conference on Artificial Intelligence*, vol.39, no.21, pp.22704-22713, 2025.

[53] F. Xu, D. Chen, T. Jia, et al, "CBDMoE: Consistent-but-diverse mixture of experts for domain generalization," *IEEE Transactions on Multimedia*, vol.26, pp.9814-9824, 2024.

[54] X. Zhai, J. Puigcerver, A. Kolesnikov, et al, "A large-scale study of representation learning with the visual task adaptation benchmark," 2019, *arXiv:1910.04867*. [Online]. Available: <https://arxiv.org/abs/1910.04867>

[55] Y. Zha, J. Wang, T. Dai, et al, "Instance-aware dynamic prompt tuning for pre-trained point cloud models," in *Proceedings of the IEEE/CVF International Conference on Computer Vision (ICCV)*, pp.14161-14170, 2023.

[56] D. Liang, T. Feng, X. Zhou, et al, "Parameter-efficient fine-tuning in spectral domain for point cloud learning," *IEEE Transactions on Pattern Analysis and Machine Intelligence*, vol.47, no.12, pp.10949-10966, 2025.

[57] Z. Wu, S. Song, A. Khosla, et al, "3D shapenets: A deep representation for volumetric shapes," in *Proceedings of the IEEE Conference on Computer Vision and Pattern Recognition (CVPR)*, pp.1912-1920, 2015.

[58] M.A. Uy, Q.H. Pham, B. Hua, et al, "Revisiting point cloud classification: A new benchmark dataset and classification model on real-world data," in *Proceedings of the IEEE/CVF Conference on Computer Vision and Pattern Recognition (CVPR)*, pp.1588-1597, 2019.

[59] L. Yi, V.G. Kim, D. Ceylan, et al, "A scalable active framework for region annotation in 3d shape collections," *ACM Transactions on Graphics*, vol.35, no.6, pp.1-12, 2016.

[60] X. Yu, L. Tang, Y. Rao, et al, "Point-bert: Pre-training 3D point cloud transformers with masked point modeling," in *Proceedings of the IEEE/CVF Conference on Computer Vision and Pattern Recognition (CVPR)*, pp.19313-19322, 2022.

[61] Y. Pang, W. Wang, E. Tay, et al, "Masked autoencoders for point cloud self-supervised learning," in *Proceedings of the European Conference on Computer Vision (ECCV)*, pp.604-621, 2022.

[62] Z. Qi, R. Dong, G. Fan, et al, "Contrast with reconstruct: Contrastive 3D representation learning guided by generative pretraining," in *Proceedings of the International Conference on Machine Learning (ICML)*, pp.28223-28243, 2023.

[63] Y. Tang, R. Zhang, Z. Guo, et al, "Point-peft: Parameter-efficient fine-tuning for 3D pre-trained models," in *Proceedings of the AAAI Conference on Artificial Intelligence*, vol.38, no.6, pp.5171-5179, 2024.

[64] S. Wang, X. Liu, L. Kong, et al, "PointLoRA: Low-rank adaptation with token selection for point cloud learning," in *Proceedings of the IEEE/CVF Conference on Computer Vision and Pattern Recognition (CVPR)*, pp.6605-6615, 2025.